NANO LETTERS
Letter
Cite This: Nano Lett. 2019, 19, 1044−1051
pubs.acs.org/NanoLett



# Nonlinear Diffraction in Asymmetric Dielectric Metasurfaces

Jonathan Bar-David and Uriel Levy*

Department of Applied Physics, The Benin School of Engineering and Computer Science, The Center for Nanoscience and Nanotechnology, The Hebrew University of Jerusalem, Jerusalem, 91904 Israel

**ABSTRACT:** Metasurfaces provide new and promising mechanisms with which to control and manipulate light at the nanoscale. While most metasurfaces are designed to operate in the linear regime, it was recently shown that such metasurfaces may also generate nonlinear signals by manipulation of the higher-order susceptibility terms. As such, metasurfaces can generate additional harmonics without the need for light propagation, as typically occurs in nonlinear crystals. While such demonstrations typically rely on the nonlinear properties of metals, we hereby report the design, fabrication, and experimental characterization of a resonant dielectric metasurface made of amorphous silicon to create and manipulate second harmonic light and control its diffraction patterns. As shown in the paper, the second harmonic generation of light follows selection rules that rely on the asymmetry of the meta-atom. Given the fact that silicon crystals are centrosymmetric, the generation of the second harmonic signal in amorphous silicon is intriguing. In fact, the second harmonic signal is generated mostly from the surface of the meta-atom. It is the use of nanostructures that increases the surface-to-volume ratio and enables second harmonic generation. Additionally, the meta-atom is designed to exploit its spectral resonances in the principal and the second harmonic frequencies for providing electromagnetic field enhancement, which assists in boosting the generation of second harmonic signals.

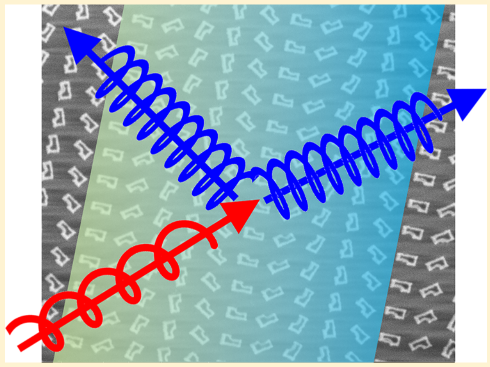

**KEYWORDS:** *Metasurfaces, dielectric metasurfaces, nonlinear optics, phase-gradient metasurfaces*

Metasurfaces, which are nanopatterned interfaces with artificial and engineered optical properties, enable the control of light's properties (namely, amplitude, phase, polarization, and frequency response).[1−22] Metasurfaces can be divided by their optical response into two main categories (namely, resonant and non-resonant metasurface), where the resonance is the characteristic of the basic nanoelement of which the metasurface is made.[1,2,23] While in non-resonant metasurfaces, the basic element is often a sub-wavelength periodic grating,[3,5,17,18,23−25] resonant metasurfaces are usually composed of discrete basic nanostructures coined "meta-atoms", which are duplicated to cover the entire surface.[1,21,26−30] In this case, the optical properties of the metasurface are dependent on the optical properties of these basic elements. For sub-wavelength particles such as meta-atoms, the optical properties are resulting from the size, shape, and the dielectric function of the material. This set of parameters controls their Mie eigenmodes and resonant frequencies.[1,7,19−21,26,28,31] Recently, there has been much interest in dielectric metasurfaces using dielectric meta-atoms due to variety of optical phenomena that they facilitate, their relative ease of fabrication, and their robustness and resilience to high optical power.[2,13,13,14,32−40]

Of light's basic properties, frequency manipulating is particularly challenging, usually requiring a strong interaction between light and a medium, to obtain (or discard) excess energy and momentum.[7,11,29,35,38,41−53] Here, we focus the discussion on the phenomena of second harmonic generation (SHG), i.e., frequency doubling. First reported in bulk medium in 1961,[54] SHG is the lowest order nonlinear process, depending on the second-order susceptibility of the material ($\chi_2$). Because $\chi_2$ interactions are usually weak, SHG normally requires complex, tailor-made crystals with low-symmetry crystal unit-cells, such as crystalline barium borate (BBO) or lithium niobate ($LiNbO_3$), to name a couple of popular, commercially available examples. Metasurfaces, the optical properties of which can be easily engineered and tailored to the specific application, are promising candidates for future nonlinear applications, and indeed, recent publications show that such metasurfaces can be used to create artificial materials with high effective $\chi_2$ and higher-order nonlinear susceptibilities, mostly in metallic-based metasurfaces.[6,35,38,50,55−58]

In this work, we design, fabricate, and experimentally characterize metasurfaces made of amorphous silicon and specifically demonstrate SHG in such structure, thus showing the surprising ability of metasurfaces to extract nonlinear processes from materials of relatively low nonlinear susceptibilities.[59,60] We further investigate the role of meta-atom symmetry in setting the selection rules to support SHG in these structures.

**Background.** For successfully generating nonlinear processes in nanostructures, and particularly for the case of SHG,

**Received:** October 28, 2018
**Revised:** December 25, 2018
**Published:** January 4, 2019




DOI: 10.1021/acs.nanolett.8b04342
Nano Lett. 2019, 19, 1044−1051

a few conditions must be met (namely, field enhancement for the principal wavelength of excitation, spatiotemporal modal overlap between the principal and second harmonic modal fields, and efficient coupling between the SH modal fields to radiation modes).[6,29,35,61−66] Another, external condition with regard to the shape of the nanostructure itself is that, due to the origin of SHG, symmetric nanostructures are predicted to support less SHG due to the lack of dipole moment at the SH,[67] as:

$$P_{2\omega} \propto |E|^2 \quad (1)$$

In practice, therefore, to generate and manipulate SH light, one would benefit from an asymmetric structure with strong field enhancement at the principal and SH frequencies.

On top of generating SHG, asymmetric structures are beneficial for light manipulation using the geometric (or Pancharatnam−Berry) phase. In this context, the geometric phase refers to the different phases acquired by circularly polarized light as it interacts with meta-atoms rotated in the $x$−$y$ plane (where the $z$ axis is light's propagation direction).[4,5,17,25,68−70] As illustrated in Figure 1A, the geometric phase acquired by light propagating through a meta-atom rotated by angle $\theta$ is given by:

$$\phi_{\text{geo}} = 2\theta\sigma \quad (2)$$

where $\sigma = \pm 1$ is light's left- or right-circular polarization.

The geometric phase is a most powerful "knob", allowing us to locally engineer artificial bi-refringence and thus to precisely control wavefront phases. Furthermore, in the case of asymmetric meta-atoms depicted in Figure 1, the asymmetry of a meta-atom allows us additional degrees of freedom of flipping or reflecting the shape, thus providing great flexibility enhancing SHG together with controlling the diffraction pattern of the second harmonic signal via the ability to obtain phase modulation from zero to $2\pi$.

For the case of manipulating optical harmonic by the geometric phase, it has been theoretically predicted that the geometric phase behaves as:[29,67]

$$\phi_{\theta}^{N} = (N \pm 1)\theta \quad (3)$$

$$N = ml \pm 1 \quad (4)$$

where $\phi_{\theta}^{N}$ is the phase of the $N$th harmonic, obtained for a rotation angle $\theta$, $N$ is the harmonic order, $m$ is the symmetry index, and $l$ is an integer. The $\pm 1$ in the top equation denotes circular polarization preservation or conversion between the principal and SH radiation, namely:

$$\sigma^{+/-}{}_{2\omega} = \sigma^{+/-}{}_{\omega} \rightarrow \phi_{\theta}^{N} = (N - 1)\theta \quad (5)$$

for polarization preservation and

$$\sigma^{+/-}{}_{2\omega} = \sigma^{-/+}{}_{\omega} \rightarrow \phi_{\theta}^{N} = (N + 1)\theta \quad (6)$$

for polarization conversion.

As will be demonstrated, these nonlinear geometric phases are inherently different than the linear geometric phase and therefore allow us to manipulate SH light differently compared to the principal light transmitted through a metasurface.

**Materials and Methods.** Figure 1B,C displays schematically our meta-atom. It is made of an amorphous silicon (a-Si) L-shaped structure fabricated on top of a glass substrate and possesses $C_1$ symmetry to in-plane rotation. The L-shaped structure is a basic $C_1$-symmetric structure, and its design offers four degrees of freedom (namely, thickness, width, backlength, and armlength in the horizontal and vertical directions, respectively). In designing our meta-atom, we have searched for a structure that fulfills the requirements mentioned above, which translates in practice to (1) the existence of scattering modes at or near the principal and second harmonic wavelength and (2) a high modal overlap, for which we have compared our calculations with structures reported in the literature.[6,57]

Figure 2A depicts the simulated single meta-atom scattering cross-section with its pronounces scattering resonances above 800 nm, along with simulated meta-atom array transmission and the matching spectroscopic measurement. We identify the longest wavelength scattering resonance (simulated ca. 900 nm) as the first "magnetic" Mie resonance of our meta-atom.[2,13,15,31]

Figure 2B,C shows finite difference time domain (FDTD) simulation calculating the electric fields evolving in our meta atom at wavelengths of 860 and 430, respectively. These calculated fields are asymmetric, which is important for utilizing the concept of geometric phase in both principal and SH wavelengths, and a field overlap calculation (not shown) provides results that are comparable to the calculated field overlaps reported in refs 6 and 57. Once the asymmetric modal fields are verified, we next examine the actual phase obtained for our meta-atoms of $C_1$ symmetry. According to the equations presented above, with parameters $N = 2$, $m = 1$, and $l = 1$ and 3, we obtain the following phases:

$$\sigma^{+/-}{}_{2\omega} = \sigma^{+/-}{}_{\omega} \rightarrow \phi_{\theta}^{N=1\times 3-1} = \theta \quad (7)$$

$$\sigma^{+/-}{}_{2\omega} = \sigma^{-/+}{}_{\omega} \rightarrow \phi_{\theta}^{N=1\times 1+1} = 3\theta \quad (8)$$

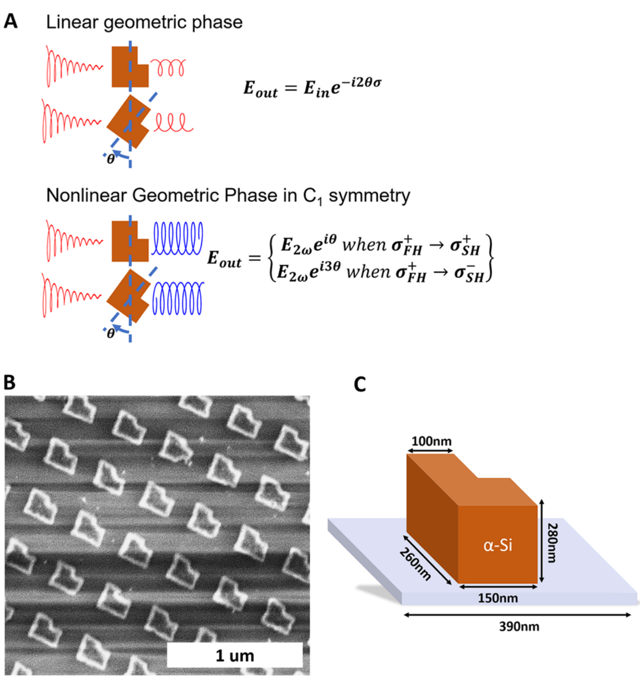


Figure 1. (A) Illustration of the geometric phase in metasurfaces. For incident light, rotating a structure by angle $\theta$ would yield a $2\theta$ phase. In the nonlinear case, the phase is governed by the harmonic order and meta-atom symmetries. (B) SEM micrograph of our fabricated L-shaped a-Si meta-atoms. (C) Illustration of meta-atom geometry. The unit-cell period is 390 nm.



DOI: 10.1021/acs.nanolett.8b04342
Nano Lett. 2019, 19, 1044−1051

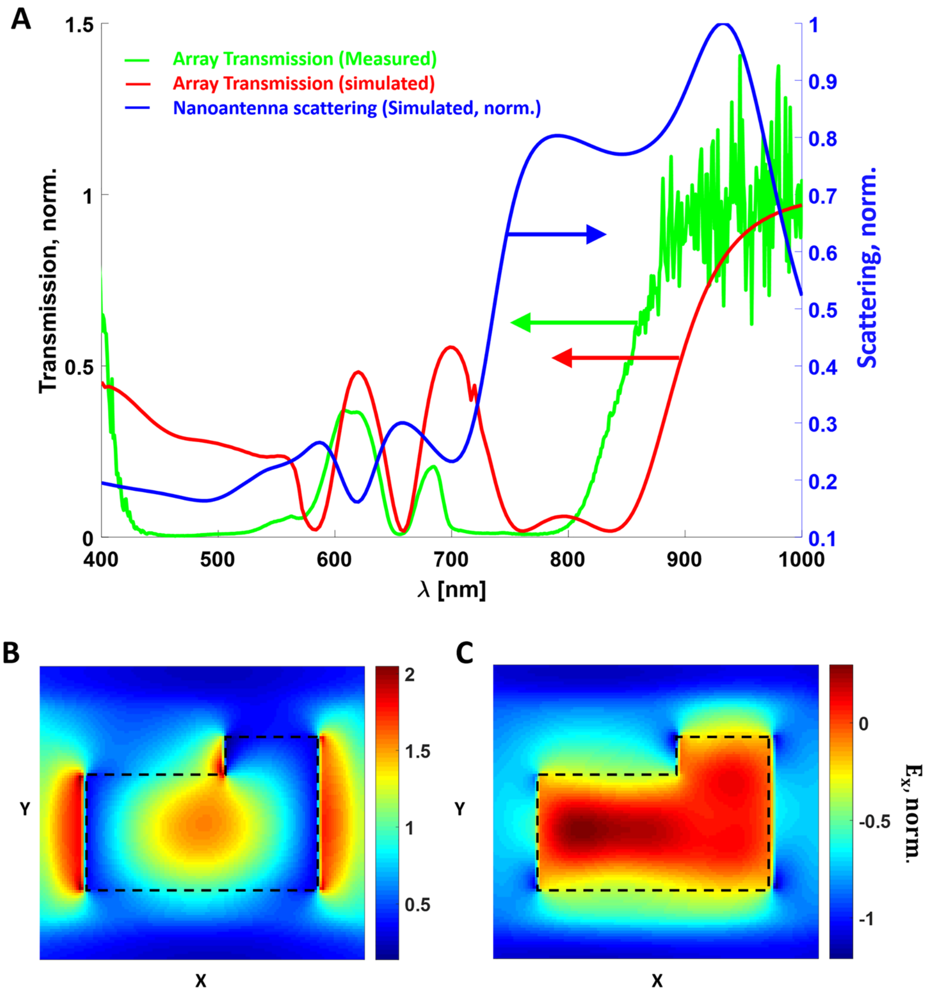


**Figure 2.** (A) Simulated (red) and measured (green) meta-atom array transmission spectrum. Differences between design and measurement are attributed to fabrication imperfections. (B, C) Simulated electric fields in the $\hat{x}$ direction for our meta-atoms at wavelengths of 860 and 430 nm, corresponding to the wavelengths of illumination and SH, respectively. The fields are given relative to the applied external field. The nanoantenna array period is 390 nm. The $n$ and $k$ values we have used were found by ellipsometry.

This result is remarkably different from the more conventional case of a geometric phase in the linear case and thus allows a clear distinction between diffraction patterns of principal and SH light.

To fabricate this structure, an a-Si layer is deposited on a glass substrate by plasma enhanced chemical vapor deposition (PECVD). Electron-beam lithography and subsequent lift-off process transfer the desired structure to a metallic protection layer atop the a-Si layer. Then, the pattern is etched into the a-Si layer by reactive ion etching (RIE), and finally, the metal layer is removed. A scanning electron microscope (SEM) micrograph of our fabricated metasurfaces are shown in Figure 1B, and a 3D illustration of the geometry is presented in Figure 1C.

Spectroscopic transmission measurements of our fabricated sample, presented in Figure 2A, show a ~50 nm line-shape shift between the designed and fabricated structures, which is attributed to size and shape variation in the fabricated sample. Still, the measured transmission reveals strong scattering for wavelengths longer than 800 nm. Based on this result, we estimate maximum scattering efficiency circa $\lambda \cong 840$ nm.

**Experimental Results.** To generate and manipulate SH light, we have fabricated a few types of metasurfaces, all consisting of identical L-shaped meta-atoms and periods of 390 nm in 200 $\mu$m × 200 $\mu$m arrays, while the meta-atom spatial orientation varies. Both principal and SH diffraction patterns were measured using a home-built microscope (depicted in Figure 3A) built around a 100× microscope objective (Olympus ULWD, NA = 0.6) and a $f$ = 300 mm singlet as tube lens. Our microscope was equipped with an extra lens for k-space (Fourier) imaging, as illustrated in Figure 3A. In this k-space imaging configuration, the conversion between the lateral coordinate on the camera and the diffraction angle is not straightforward because the k-space imaging system acts as an additional 6× magnifier. Accounting for this, the relation between lateral coordinate in the sensor plane and the diffraction angle is given by:

$$x_{\text{sensor}} = f_{\text{objective}} \times \tan(\sin^{-1}\theta_{\text{diff}}) \times M \quad (9)$$

where $x$ is the lateral coordinate, $f$ is the objective focal length ($f_{\text{objective}}$ = 1.8 mm), $\theta_{\text{diff}}$ is the diffraction angle, and $M$ is the additional k-space magnification. First, to observe SHG, we have measured an array consisting of meta-atoms, all having the same orientation, as shown in Figure 1B. The array in this experiment (and in all SHG experiment reported) was illuminated by a weakly focused beam with FWHM of ~200 $\mu$m, roughly the size of the nanoantenna array. Due to the sub-



DOI: 10.1021/acs.nanolett.8b04342
Nano Lett. 2019, 19, 1044−1051

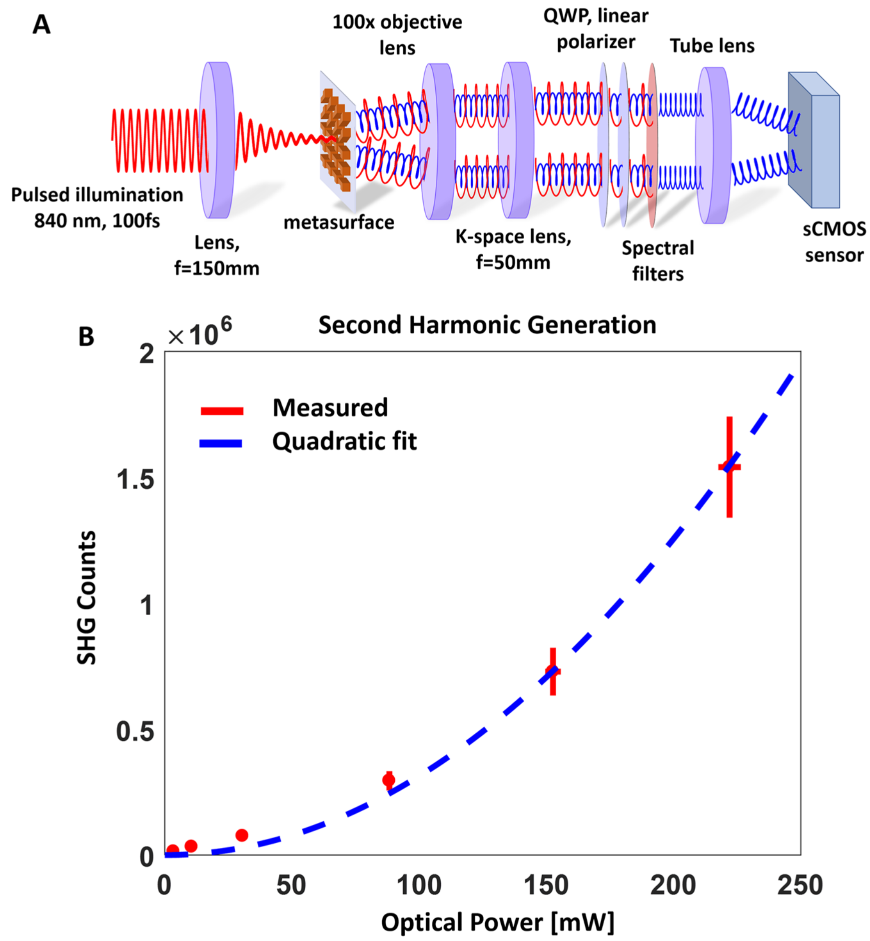


**Figure 3.** (A) Schematic illustration of the experimental setup. The sample is illuminated by a short pulse laser that is weakly focused to form a focal spot of ∼100 $\mu$m in diameter. Light is collected by a 100× objective, and k-space is imaged by a lens. The principal wavelength is filtered, and Stokes parameters are measured by rotating a polarizer and a quarter-wave plate. Diffraction patterns are recorded by sCMOS camera (Hamamatsu ORCA flash 4 version 2). (B) SHG obtained from our metasurface as a function of illumination intensity. We observed an excellent fit of the detected SHG signal to the square of the illumination power.

wavelength periodicity, combined with the use of meta-atoms with identical orientation, this array has no diffraction in the principal or SH wavelength. Due to the filtering of the principal light, the obtained k-space image consists only a single SH spot at the center. We have measured the total SH intensity while increasing principal laser power. The result (Figure 3B) shows that the measured signal is dependent upon the square of the input power, which is a validation for SHG. This is by itself an important result, as the generation of SH signal from amorphous silicon is expected to be negligible due to the centrosymmetric nature of silicon. However, when implemented as a metasurface, SH signal can be generated from the surfaces of the meta atoms and, combined with the field enhancement, an SH signal can indeed be observed.

Next, we demonstrate the ability to manipulate the SH radiation in space without diffracting the principal light. For this, we form an array with a period of 10 meta-atoms in which 5 are situated in a zero angle and 5 are rotated by 180°, as illustrated in the inset of Figure 4A. For the principal wavelength, this is a binary grating with phases 0 and $2\pi$, and thus, no diffraction is expected, as indeed shown by the measurement (Figure 4A). However, for the SH radiation, the phases of this binary grating are 0 and $\pi$ (or the equivalent $3\pi$ for polarization conversion). Therefore, the SH signal is expected to show ±1 diffraction orders at an angle of $\theta_{\text{diffraction}} = \sin^{-1}\frac{\lambda_{\text{SH}}}{\Lambda_{\text{period}}} \cong 6°$, which, according to eq 9 above translates to a distance of ∼1.1 mm from the optical axis. Indeed, the measured SH signal shows these ±1 diffraction orders alongside the zero order signal, as observed in Figure 4B. This is evidence for the inherent difference between the linear and the SH geometric phase.

Finally, we measure the nonlinear diffraction from an array of linearly varying phase, where our meta-atoms are continuously rotated across the array, as depicted in Figure 5A. This is essentially a blazed grating implemented by the concept of geometrical phase with a period of 10 meta-atoms and a phase variation from 0 to $4\pi$. For the case of geometric phase in the linear regime, this structure acts as a polarization-dependent blazed-grating, in which the direction of diffracted light is dependent upon the polarization of the incident beam of light. This is indeed observed in a linear diffraction measurement, presented in Figure 5B. Ideally, the linear diffraction of such a pattern should be symmetric (i.e., the +1 and −1 orders should be equal under opposite input polarization). The asymmetry between LCP and RCP measurements are attributed to fabrication and measurement imperfections. As can be seen, flipping the polarization shifts the diffraction orders with respect to the zero order. This observation is in agreement with previous demonstrations of


DOI: 10.1021/acs.nanolett.8b04342
Nano Lett. 2019, 19, 1044−1051

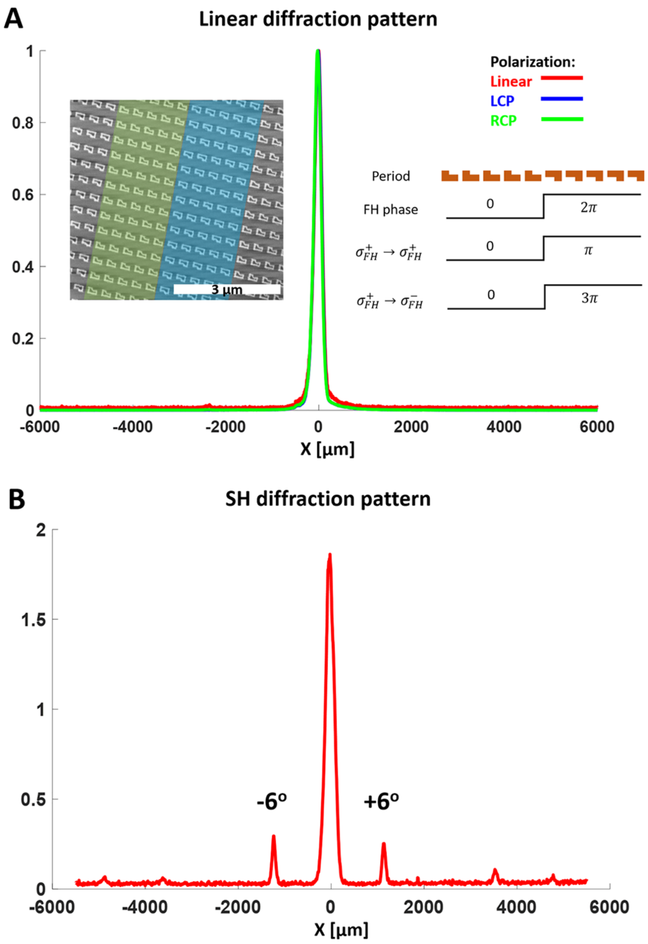


**Figure 4.** (A, left inset) SEM micrograph of a fabricated binary phase grating. The 0 and $2\pi$ phase regions are colored in green and blue, respectively. (A, right inset) Illustration explaining the different geometric phases of this structure. (A) Diffraction pattern of the principal light from the phase grating. As expected, no diffraction is observed. (B) SH diffraction from the same structure. Diffraction orders can be clearly seen. The first-order diffraction angle is ~6°, as predicted by simple diffraction calculation.

geometric-phase metasurfaces.[4,5,8,17,25] After validating the behavior of the linear geometric phase, we examine the SH diffraction from this structure, as presented in Figure 5C. As is the case for linear diffraction, the SH signal also shows polarization-dependent diffraction pattern. As can be seen, the right circular polarization (RCP) case supports negative diffraction orders, while the left circular polarization (LCP) case supports positive diffraction orders. Another interesting result of SHG in this structure is the location of diffraction orders. As can be observed from Figure 5C,D the first diffraction orders of the SH light are located at one-quarter of the distance of the first order of the principal light, and the next diffraction orders are at one-half and at three-fourths of this distance. These remarkable diffraction angles are a direct outcome of the nonlinear geometric phase of $\theta$ or $3\theta$, combined with the fact that the SH wavelength is only half of the principal wavelength.

More specifically, for linear diffraction our blazed grating has a linear phase variation between 0 and $4\pi$ (as the meta-atoms are rotated a full $2\pi$ in each period), and hence, the effective period (where phase changes between 0 and $2\pi$) is actually only 5 unit cells long, i.e., 1.95 $\mu$m. This grating period generates a diffraction angle of about ~24°for the principal wavelength around 800 nm. However, for the second harmonic light, due to the difference in geometric phase, the phases vary either between 0 and $2\pi$ (for same polarization) or from 0 to $6\pi$ (for polarization conversion). Hence, for SHG the actual grating period would be either 3.9 or 1.3 $\mu$m and the diffraction angles (for SH light having half the principal wavelength) would be ~6° or ~18° for polarization-maintaining or polarization-converting processes, respectively, i.e., one-fourth or three-fourths of the principal diffraction angle, as seen in our experimental results. The second and fourth diffraction orders are "parasitic" diffraction orders arising from phase discontinuities in the blazed structures.

To further understand the polarization content in each of the diffraction orders, we have measured the Stokes parameters of the diffracted SH light. Keeping in mind that the phase of the principal light varies as $2\theta$, and assuming, for example, RCP excitation, we are expecting to observe RCP at one-fourth of the location of the first diffraction order of the principal light (one half originates from the slower phase change and the other half originates from the wavelength of the SH signal being half of the principal wavelength) and LCP at three-fourths of the distance. This is indeed confirmed by measuring the Stokes $S_3$ parameter, displayed in Figure 5D. Here, the Stokes $S_3$ parameter (green curve) flips sign between diffraction orders one-fourth and three-fourths, indicating that these orders contain orthogonal circular polarization. This is another intriguing feature of SHG in such a structure and direct evidence for the validity of the theory presented above.

**Discussion.** in this work, we fabricate an a-Si metasurface with the goal of observing second harmonic generation and detecting light at half of the principal wavelength. Contrary to previous studies of SHG in a-Si,[59,60] here, the modal fields distribution in and around the meta-atoms play a role in generating SH radiation. Our SH conversion efficiency, estimated at $10^{-14}$, is low compared with state-of-the-art efficiencies in metals ($10^{-10}$)[6,50,57] or the superior efficiency of III−V materials (reported up to $10^{-3}$).[35,56,71] Nonetheless, we were able to explore the importance of selection rules in establishing SHG. As shown, meta-atom design, resonances, and symmetries are of utmost importance for the control of light in both near- and far-field. Here, the $C_1$ symmetry is what enables the unique manipulation of light, unobtainable for symmetric meta-atom design. It should be mentioned that we do not observe third harmonic generation (THG) due to the relatively long pulse duration and the THG being at the UV regime beyond the sensitivity of our detector.

An interesting question arising from these experiments is the role of symmetry in geometric-phase related processes because symmetry is often linked to conservation laws. In the SHG process, we can easily understand the conservation of energy and linear momentum. However, angular momentum is not conserved in these processes[72] due to a torque applied by the structure. So far, we are not aware of rigorous consideration of angular momentum conservation in linear and nonlinear geometric-phase phenomena. In the special case of C1 symmetry, there seem to be no constraints arising from angular momentum on SHG processes. The only constraint arises directly from the meta-atom symmetry, allowing for SHG in all polarizations, as predicted theoretically.[67] This is among the causes for the large zero diffraction orders seen in our measurements (for example, Figure 4B−D).


DOI: 10.1021/acs.nanolett.8b04342
Nano Lett. 2019, 19, 1044−1051

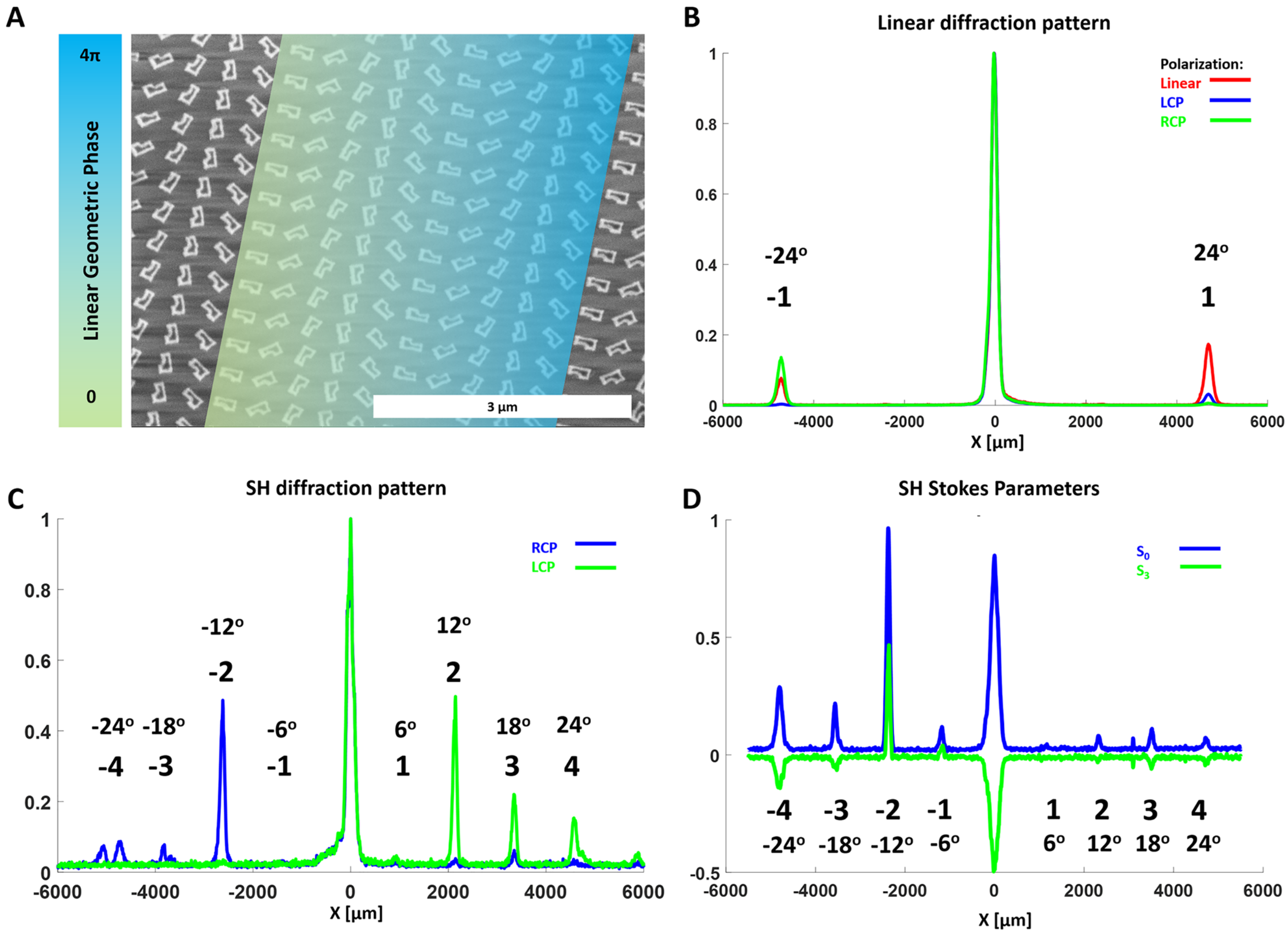


**Figure 5.** (A) SEM micrograph of a blazed phase grating with linear geometric phase varying from 0 to $4\pi$. (B) Linear diffraction pattern from this grating. Different circular polarizations create the ±1 diffraction orders denoted by numbers. The first-order diffraction angle is ∼24°, which matches the prediction of simple diffraction theory. (C) SH diffraction of this structure. The polarization dependence of SH light and the nonlinear geometric phase are validated by this unusual diffraction pattern. It is easy to notice that the 1st SH diffraction order is at a distance of one-quarter of the distance of the 1st linear diffraction order, which corresponds to a diffraction angle of ∼6°. (D) Measurement of the Stokes' parameters for SHG by RCP principal light. The sign inversion between the first and third diffraction orders is solid proof for the different phases of spin-maintaining and spin-changing SHG processes.

On top of being able to demonstrate SHG, we also show that the concept of the geometric phase is valid for harmonic-generation as well as for other nonlinear properties. As discussed in the paper, the obtained nonlinear geometric phase is different from the linear phase. In this context, we validate the theoretical prediction for $C_1$ symmetry,[67] which, to the best of our knowledge, does not appear in nature and can be achieved only by man-made structures such as metasurfaces and metamaterials.

## AUTHOR INFORMATION


### Corresponding Author

*E-mail: ulevy@mail.huji.ac.il.

### ORCID

Jonathan Bar-David: 0000-0002-4464-636X
Uriel Levy: 0000-0002-5918-1876


### Notes

The authors declare no competing financial interest.

## ACKNOWLEDGMENTS

We acknowledge funding from the Israeli ministry of science and technology. J.B.D. acknowledges the support of the applied research scholarship of the Israeli ministry of science and technology.

## REFERENCES


(1) Novotny, L.; van Hulst, N. Antennas for Light. *Nat. Photonics* **2011**, *5* (2), 83−90.

(2) Kuznetsov, A. I.; Miroshnichenko, A. E.; Brongersma, M. L.; Kivshar, Y. S.; Luk'yanchuk, B. Optically Resonant Dielectric Nanostructures. *Science* **2016**, *354* (6314), aag2472.

(3) Lalanne, P. Waveguiding in Blazed-Binary Diffractive Elements. *J. Opt. Soc. Am. A* **1999**, *16* (10), 2517−2520.

(4) Bomzon, Z.; Kleiner, V.; Hasman, E. Pancharatnam−Berry Phase in Space-Variant Polarization-State Manipulations with Subwavelength Gratings. *Opt. Lett.* **2001**, *26* (18), 1424−1426.

(5) Levy, U.; Tsai, C.-H.; Kim, H.-C.; Fainman, Y. Design, Fabrication and Characterization of Subwavelength Computer-Generated Holograms for Spot Array Generation. *Opt. Express* **2004**, *12* (22), 5345−5355.




DOI: 10.1021/acs.nanolett.8b04342
*Nano Lett.* 2019, 19, 1044−1051

(6) Segal, N.; Keren-Zur, S.; Hendler, N.; Ellenbogen, T. Controlling Light with Metamaterial-Based Nonlinear Photonic Crystals. *Nat. Photonics* **2015**, *9* (3), 180−184.
(7) Salomon, A.; Zielinski, M.; Kolkowski, R.; Zyss, J.; Prior, Y. Size and Shape Resonances in Second Harmonic Generation from Silver Nanocavities. *J. Phys. Chem. C* **2013**, *117*, 22377.
(8) Xu, F.; Cheng, C.-C.; Scherer, A.; Tyan, R.-C.; Sun, P.-C.; Fainman, Y. Fabrication, Modeling, and Characterization of Form-Birefringent Nanostructures. *Opt. Lett.* **1995**, *20* (24), 2457−2459.
(9) Yeh, P.; Yariv, A.; Cho, A. Y. Optical Surface Waves in Periodic Layered Media. *Appl. Phys. Lett.* **1978**, *32* (2), 104−105.
(10) Zhu, X.; Vannahme, C.; Højlund-Nielsen, E.; Mortensen, N. A.; Kristensen, A. Plasmonic Colour Laser Printing. *Nat. Nanotechnol.* **2016**, *11* (4), 325−329.
(11) Metzger, B.; Hentschel, M.; Lippitz, M.; Giessen, H. Third-Harmonic Spectroscopy and Modeling of the Nonlinear Response of Plasmonic Nanoantennas. *Opt. Lett.* **2012**, *37* (22), 4741−4743.
(12) O'Brien, K.; Suchowski, H.; Rho, J.; Salandrino, A.; Kante, B.; Yin, X.; Zhang, X. Predicting Nonlinear Properties of Metamaterials from the Linear Response. *Nat. Mater.* **2015**, *14* (4), 379−383.
(13) Decker, M.; Staude, I.; Falkner, M.; Dominguez, J.; Neshev, D. N.; Brener, I.; Pertsch, T.; Kivshar, Y. S. High-Efficiency Dielectric Huygens' Surfaces. *Adv. Opt. Mater.* **2015**, *3* (6), 813−820.
(14) Staude, I.; Miroshnichenko, A. E.; Decker, M.; Fofang, N. T.; Liu, S.; Gonzales, E.; Dominguez, J.; Luk, T. S.; Neshev, D. N.; Brener, I.; et al. Tailoring Directional Scattering through Magnetic and Electric Resonances in Subwavelength Silicon Nanodisks. *ACS Nano* **2013**, *7* (9), 7824−7832.
(15) Iyer, P. P.; Butakov, N. A.; Schuller, J. A. Reconfigurable Semiconductor Phased-Array Metasurfaces. *ACS Photonics* **2015**, *2*, 1077.
(16) Chong, K. E.; Hopkins, B.; Staude, I.; Miroshnichenko, A. E.; Dominguez, J.; Decker, M.; Neshev, D. N.; Brener, I.; Kivshar, Y. S. Observation of Fano Resonances in All-Dielectric Nanoparticle Oligomers. *Small* **2014**, *10* (10), 1985−1990.
(17) Desiatov, B.; Mazurski, N.; Fainman, Y.; Levy, U. Polarization Selective Beam Shaping Using Nanoscale Dielectric Metasurfaces. *Opt. Express* **2015**, *23* (17), 22611−22618.
(18) Yu, N.; Capasso, F. Flat Optics with Designer Metasurfaces. *Nat. Mater.* **2014**, *13* (2), 139−150.
(19) Mie, G. Beiträge Zur Optik Trüber Medien, Speziell Kolloidaler Metallösungen. *Ann. Phys.* **1908**, *330* (3), 377−445.
(20) Jackson, J. D. *Classical Electrodynamics*, 3rd ed.; Wiley: New York, NY, 1999.
(21) Genet, C.; Ebbesen, T. W. Light in Tiny Holes. *Nature* **2007**, *445* (7123), 39−46.
(22) Ebbesen, T. W.; Lezec, H. J.; Ghaemi, H. F.; Thio, T.; Wolff, P. A. Extraordinary Optical Transmission through Sub-Wavelength Hole Arrays. *Nature* **1998**, *391* (6668), 667−669.
(23) Lin, D.; Fan, P.; Hasman, E.; Brongersma, M. L. Dielectric Gradient Metasurface Optical Elements. *Science* **2014**, *345* (6194), 298−302.
(24) Lalanne, P.; Chavel, P. Metalenses at Visible Wavelengths: Past, Present, Perspectives. *Laser & Photonics Rev.* **2017**.111600295
(25) Bar-David, J.; Stern, L.; Levy, U. Dynamic Control over the Optical Transmission of Nanoscale Dielectric Metasurface by Alkali Vapors. *Nano Lett.* **2017**, *17* (2), 1127−1131.
(26) Meinzer, N.; Barnes, W. L.; Hooper, I. R. Plasmonic Meta-Atoms and Metasurfaces. *Nat. Photonics* **2014**, *8* (12), 889−898.
(27) Luk'yanchuk, B.; Zheludev, N. I.; Maier, S. A.; Halas, N. J.; Nordlander, P.; Giessen, H.; Chong, C. T. The Fano Resonance in Plasmonic Nanostructures and Metamaterials. *Nat. Mater.* **2010**, *9* (9), 707−715.
(28) Kuznetsov, A. I.; Miroshnichenko, A. E.; Fu, Y. H.; Zhang, J.; Luk'yanchuk, B. *Sci. Rep.* **2012**, *2*, 492.
(29) Li, G.; Chen, S.; Pholchai, N.; Reineke, B.; Wong, P. W. H.; Pun, E. Y. B.; Cheah, K. W.; Zentgraf, T.; Zhang, S. Continuous Control of the Nonlinearity Phase for Harmonic Generations. *Nat. Mater.* **2015**, *14* (6), 607−612.
(30) Zhu, X.; Yan, W.; Levy, U.; Mortensen, N. A.; Kristensen, A. Resonant Laser Printing of Structural Colors on High-Index Dielectric Metasurfaces. *Sci. Adv.* **2017**, *3* (5), e1602487−e1602487.
(31) Lewi, T.; Iyer, P. P.; Butakov, N. A.; Mikhailovsky, A. A.; Schuller, J. A. Widely Tunable Infrared Antennas Using Free Carrier Refraction. *Nano Lett.* **2015**, *15* (12), 8188−8193.
(32) Barsukova, M. G.; Shorokhov, A. S.; Musorin, A. I.; Neshev, D. N.; Kivshar, Y. S.; Fedyanin, A. A. Magneto-Optical Response Enhanced by Mie Resonances in Nanoantennas. *ACS Photonics* **2017**, *4*, 2390.
(33) Hopkins, B.; Filonov, D. S.; Miroshnichenko, A. E.; Monticone, F.; Alù, A.; Kivshar, Y. S. Interplay of Magnetic Responses in All-Dielectric Oligomers To Realize Magnetic Fano Resonances. *ACS Photonics* **2015**, *2* (6), 724−729.
(34) Bar-David, J.; Mazurski, N.; Levy, U. In-Situ Planarization of Huygens Metasurfaces by Nanoscale Local Oxidation of Silicon. *ACS Photonics* **2017**, *4*, 2359.
(35) Shcherbakov, M. R.; Neshev, D. N.; Hopkins, B.; Shorokhov, A. S.; Staude, I.; Melik-Gaykazyan, E. V.; Decker, M.; Ezhov, A. A.; Miroshnichenko, A. E.; Brener, I.; et al. Enhanced Third-Harmonic Generation in Silicon Nanoparticles Driven by Magnetic Response. *Nano Lett.* **2014**, *14* (11), 6488−6492.
(36) Vaskin, A.; Bohn, J.; Chong, K. E.; Bucher, T.; Zilk, M.; Choi, D.-Y.; Neshev, D. N.; Kivshar, Y. S.; Pertsch, T.; Staude, I. Directional and Spectral Shaping of Light Emission with Mie-Resonant Silicon Nanoantenna Arrays. *ACS Photonics* **2018**, *5*, 1359.
(37) Brener, I.; Miao, X.; Shaner, E. A.; Passmore, B. S.; Jun, Y. C. *Mid-Infrared Tunable Metamaterials*. US. Patent US9018642, April 28, 2015.
(38) Campione, S.; Benz, A.; Sinclair, M. B.; Capolino, F.; Brener, I. Second Harmonic Generation from Metamaterials Strongly Coupled to Intersubband Transitions in Quantum Wells. *Appl. Phys. Lett.* **2014**, *104* (13), 131104.
(39) Campione, S.; Liu, S.; Basilio, L. I.; Warne, L. K.; Langston, W. L.; Luk, T. S.; Wendt, J. R.; Reno, J. L.; Keeler, G. A.; Brener, I.; et al. Broken Symmetry Dielectric Resonators for High Quality Factor Fano Metasurfaces. *ACS Photonics* **2016**, *3* (12), 2362−2367.
(40) Jahani, S.; Jacob, Z. All-Dielectric Metamaterials. *Nat. Nanotechnol.* **2016**, *11* (1), 23−36.
(41) Agarwal, G. S.; Jha, S. S. Theory of Second Harmonic Generation at a Metal Surface with Surface Plasmon Excitation. *Solid State Commun.* **1982**, *41* (6), 499−501.
(42) Bar-Lev, D.; Scheuer, J. Efficient Second Harmonic Generation Using Nonlinear Substrates Patterned by Nano-Antenna Arrays. *Opt. Express* **2013**, *21* (24), 29165−29178.
(43) Bernasconi, G. D.; Butet, J.; Martin, O. J. F. Mode Analysis of Second-Harmonic Generation in Plasmonic Nanostructures. *J. Opt. Soc. Am. B* **2016**, *33* (4), 768−779.
(44) Bozhevolnyi, S. I.; Pedersen, K. Second Harmonic Generation Due to Surface Plasmon Localization. *Surf. Sci.* **1997**, *377−379*, 384−387.
(45) Butet, J.; Russier-Antoine, I.; Jonin, C.; Lascoux, N.; Benichou, E.; Martin, O. J. F.; Brevet, P.-F. Universal Scaling of Plasmon Coupling in Metal Nanostructures: Checking the Validity for Higher Plasmonic Modes Using Second Harmonic Generation. *Phys. Rev. B: Condens. Matter Mater. Phys.* **2013**, *87* (23), 235437.
(46) Ginzburg, P.; Krasavin, A.; Sonnefraud, Y.; Murphy, A.; Pollard, R. J.; Maier, S. A.; Zayats, A. V. Nonlinearly Coupled Localized Plasmon Resonances: Resonant Second-Harmonic Generation. *Phys. Rev. B: Condens. Matter Mater. Phys.* **2012**, *86* (8), 085422.
(47) Metzger, B.; Schumacher, T.; Hentschel, M.; Lippitz, M.; Giessen, H. Third Harmonic Mechanism in Complex Plasmonic Fano Structures. *ACS Photonics* **2014**, *1*, 471.
(48) Metzger, B.; Hentschel, M.; Nesterov, M.; Schumacher, T.; Lippitz, M.; Giessen, H. Nonlinear Optics of Complex Plasmonic Structures: Linear and Third-Order Optical Response of Orthogonally Coupled Metallic Nanoantennas. *Appl. Phys. B: Lasers Opt.* **2016**, *122* (4), 1−9.



DOI: 10.1021/acs.nanolett.8b04342
*Nano Lett.* 2019, 19, 1044−1051

(49) Smirnova, D. A.; Khanikaev, A. B.; Smirnov, L. A.; Kivshar, Y. S. Multipolar Third-Harmonic Generation Driven by Optically-Induced Magnetic Resonances. *ACS Photonics* **2016**, *3* (8), 1468−1476.

(50) Almeida, E.; Bitton, O.; Prior, Y. Nonlinear Metamaterials for Holography. *Nat. Commun.* **2016**, *7*, 12533.

(51) Almeida, E.; Shalem, G.; Prior, Y. Subwavelength Nonlinear Phase Control and Anomalous Phase Matching in Plasmonic Metasurfaces. *Nat. Commun.* **2016**, *7*, 10367.

(52) Kauranen, M.; Zayats, A. V. Nonlinear Plasmonics. *Nat. Photonics* **2012**, *6* (11), 737−748.

(53) Ding, F.; Pors, A.; Bozhevolnyi, S. I. Gradient Metasurfaces: A Review of Fundamentals and Applications. *Rep. Prog. Phys.* **2018**, *81* (2), 026401.

(54) Franken, P. A.; Hill, A. E.; Peters, C. W.; Weinreich, G. Generation of Optical Harmonics. *Phys. Rev. Lett.* **1961**, *7* (4), 118−119.

(55) Chen, S.; Rahmani, M.; Li, K. F.; Miroshnichenko, A.; Zentgraf, T.; Li, G.; Neshev, D.; Zhang, S. Third Harmonic Generation Enhanced by Multipolar Interference in Complementary Silicon Metasurfaces. *ACS Photonics* **2018**, *5*, 1671.

(56) Vabishchevich, P. P.; Liu, S.; Sinclair, M. B.; Keeler, G. A.; Peake, G. M.; Brener, I. Enhanced Second-Harmonic Generation Using Broken Symmetry III−V Semiconductor Fano Metasurfaces. *ACS Photonics* **2018**, *5* (5), 1685−1690.

(57) Keren-Zur, S.; Avayu, O.; Michaeli, L.; Ellenbogen, T. Nonlinear Beam Shaping with Plasmonic Metasurfaces. *ACS Photonics* **2016**, *3* (1), 117−123.

(58) Wolf, O.; Campione, S.; Benz, A.; Ravikumar, A. P.; Liu, S.; Luk, T. S.; Kadlec, E. A.; Shaner, E. A.; Klem, J. F.; Sinclair, M. B.; et al. Phased-Array Sources Based on Nonlinear Metamaterial Nanocavities. *Nat. Commun.* **2015**, *6*, 7667.

(59) Alexandrova, S.; Danesh, P.; Maslyanitsyn, I. A. Second Harmonic Generation in Hydrogenated Amorphous Silicon. *Phys. Rev. B: Condens. Matter Mater. Phys.* **2000**, *61* (16), 11136−11138.

(60) Kessels, W. M. M.; Gielis, J. J. H.; Aarts, I. M. P.; Leewis, C. M.; van de Sanden, M. C. M. Spectroscopic Second Harmonic Generation Measured on Plasma-Deposited Hydrogenated Amorphous Silicon Thin Films. *Appl. Phys. Lett.* **2004**, *85* (18), 4049−4051.

(61) Ginzburg, P.; Hayat, A.; Berkovitch, N.; Orenstein, M. Nonlocal Ponderomotive Nonlinearity in Plasmonics. *Opt. Lett.* **2010**, *35* (10), 1551−1553.

(62) Celebrano, M.; Wu, X.; Baselli, M.; Großmann, S.; Biagioni, P.; Locatelli, A.; De Angelis, C.; Cerullo, G.; Osellame, R.; Hecht, B.; et al. *Mode-Matching in Multiresonant Plasmonic Nanoantennas for Enhanced Second Harmonic Generation*. 2014, ArXiv14120698 Cond-Mat Physics. arXiv.org e-print archive. https://arxiv.org/pdf/1412.0698v2 (accessed).

(63) Thyagarajan, K.; Rivier, S.; Lovera, A.; Martin, O. J. F. Enhanced Second-Harmonic Generation from Double Resonant Plasmonic Antennae. *Opt. Express* **2012**, *20* (12), 12860−12865.

(64) Mayergoyz, I. D.; Fredkin, D. R.; Zhang, Z. Electrostatic (Plasmon) Resonances in Nanoparticles. *Phys. Rev. B: Condens. Matter Mater. Phys.* **2005**, *72* (15), 155412.

(65) Kruk, S.; Weismann, M.; Bykov, A. Y.; Mamonov, E. A.; Kolmychek, I. A.; Murzina, T.; Panoiu, N. C.; Neshev, D. N.; Kivshar, Y. S. Enhanced Magnetic Second-Harmonic Generation from Resonant Metasurfaces. *ACS Photonics* **2015**, *2*, 1007.

(66) Wang, L.; Kruk, S.; Xu, L.; Rahmani, M.; Smirnova, D.; Solntsev, A.; Kravchenko, I.; Neshev, D.; Kivshar, Y. Shaping the Third-Harmonic Radiation from Silicon Nanodimers. *Nanoscale* **2017**, *9* (6), 2201−2206.

(67) Bhagavantam, S.; Chandrasekhar, P. Harmonic Generation and Selection Rules in Nonlinear Optics. *Proc. - Indian Acad. Sci., Sect. A* **1972**, *76* (1), 13−20.

(68) Bomzon, Z.; Biener, G.; Kleiner, V.; Hasman, E. Space-Variant Pancharatnam−Berry Phase Optical Elements with Computer-Generated Subwavelength Gratings. *Opt. Lett.* **2002**, *27* (13), 1141−1143.

(69) Bliokh, K. Y.; Gorodetski, Y.; Kleiner, V.; Hasman, E. Coriolis Effect in Optics: Unified Geometric Phase and Spin-Hall Effect. *Phys. Rev. Lett.* **2008**, *101* (3), 030404 DOI: 10.1103/PhysRevLett.101.030404.

(70) Devlin, R. C.; Ambrosio, A.; Wintz, D.; Oscurato, S. L.; Zhu, A. Y.; Khorasaninejad, M.; Oh, J.; Maddalena, P.; Capasso, F. Spin-to-Orbital Angular Momentum Conversion in Dielectric Metasurfaces. *Opt. Express* **2017**, *25*, 4239.

(71) Neshev, D. N. Nonlinear Wave Mixing in Semiconductor Nanoantennas and Metasurfaces. In *Conference on Lasers and Electro-Optics*; Optical Society of America: Washington, DC, 2018.

(72) Neale, S. L.; MacDonald, M. P.; Dholakia, K.; Krauss, T. F. All-Optical Control of Microfluidic Components Using Form Birefringence. *Nat. Mater.* **2005**, *4* (7), 530−533.




DOI: 10.1021/acs.nanolett.8b04342
*Nano Lett.* 2019, 19, 1044−1051